Available online at www.sciencedirect.com
ScienceDirect
Journal of Sound and Vibration 310 (2008) 1093–1111
JOURNAL OF SOUND AND VIBRATION
www.elsevier.com/locate/jsvi

A systematic method to obtain 3D finite-difference formulations for acoustic intensity and other energy quantities

Jean-Claude Pascal[a,*], Jing-Fang Li[b]

[a]*Laboratoire d'Acoustique de l'Université du Maine (CNRS UMR 6613) and Ecole Nationale Supérieure d'Ingénieurs du Mans (ENSIM), Université du Maine, rue Aristote, 72000 Le Mans, France*
[b]*Visual VibroAcoustics, 51 rue d'Alger, 72000 Le Mans, France*

Received 9 November 2006; received in revised form 17 August 2007; accepted 21 August 2007

Abstract

A systematic method is described to obtain formulations based on the finite-difference approximation for computation of the energy quantities of three-dimensional (3D)-sound fields from measurements. It uses up to the first-order terms of the Taylor series expansion of the sound pressure about the microphone positions of a particular probe configuration. The use of a symbolic computation allows approximate expressions to be obtained for all energy quantities as a function of the cross-spectral densities of the microphone signals. The application of this approach is illustrated by the three components of the active acoustic intensity vector and the energy densities for different types of 3D-probes consisting of 4–6 microphones. The inherent effect associated with the finite-sum and finite-difference approximations is evaluated for each of these probes by considering 1D sound fields in order to make a comparison of their performance.

1. Introduction

The finite-difference technique between two sensors is used to obtain the gradients of acoustic and vibration fields, which are essential for the calculation of sound intensity (density of energy flow) and energy density from measurement data. Soon after the publications of Fahy [1] and Pavic [2], this technique became very popular in the 1980s and has been the basis of instruments for sound intensity measurements since. It has been used to measure the energy density, for example, by Elko [3] and then more recently by Cazzolato and Hansen [4]. Simple and obvious for the one-dimensional (1D) probes, the approximate formulations of the energy quantities become much more complicated for different configurations of 3D-probes. Moreover, a probe found in some publications with the same configuration can be oriented differently in the Cartesian coordinate system and the identification number of each microphone can be modified. The methods used to obtain the practical formulations for determination of sound quantities are not very explicit in the literature [5]. Some authors [6] interpolate the sound pressure at virtual points between the microphones, in order to then apply the approximation for the gradient in a direction by the difference of the pressures between the two virtual

*Corresponding author.
E-mail addresses: Jean-Claude.Pascal@univ-lemans.fr (J.-C. Pascal), Jingfang.Li@VisualVibroAcoustics.com (J.-F. Li).

0022-460X/$ - see front matter © 2007 Elsevier Ltd. All rights reserved.
doi:10.1016/j.jsv.2007.08.029

points. It then remains a tedious calculation to be made that allows the practical formulations to be written in terms of the cross-spectral power densities between microphone signals.

This article shows how it is possible to use a systematic approach and symbolic computational tools to easily obtain the finite-sum and finite-difference approximation formulations and compute the energetic quantities in sound fields from measurements using multi-microphone probes and multichannel FFT analysers. Without wanting to be exhaustive, some formulations for 4–6-microphone probe configurations listed in Appendix A are obtained to illustrate the method and compared by considering the difference-and-sum inherent error caused by the high-frequency measurement limitations.

2. Principle of the method

The complex acoustic intensity $\mathbf{\Pi}$ and the total acoustic energy density E in a medium without flow are expressed by the complex pressure p and complex particle velocity $\mathbf{u}$ in the following forms:

$$\mathbf{\Pi} = \mathbf{I} + \mathrm{j}\mathbf{J} = \frac{1}{2} p\mathbf{u}^* \quad \text{and} \quad E = V + T = \frac{|p|^2}{4\rho_0 c^2} + \frac{\rho_0}{4}\mathbf{u}\cdot\mathbf{u}^*, \tag{1}$$

where $\mathbf{I}$ and $\mathbf{J}$ are, respectively, active and reactive intensities, ρ_0 is the mass density of the fluid, c the speed of sound. V and T are the potential and kinetic energy densities, respectively. The superscript * denotes the complex conjugate and $|p|$ is the modulus of the complex pressure. The particle velocity is expressed in terms of the gradient of the pressure according to Euler's equation

$$\mathbf{u} = \frac{\mathrm{j}}{\rho_0\omega}\nabla p, \tag{2}$$

where $\omega = 2\pi f$ is the angular frequency, with f being the frequency in Hz. A more complete and general representation of energy quantities of sound fields can be obtained by the definition of the *field matrix* [7] that is written as

$$\mathbf{F} = \frac{1}{2}\mathbf{\Theta}\mathbf{\Theta}^{\mathrm{H}} = \begin{bmatrix} 2cV & \Pi_x & \Pi_y & \Pi_z \\ \Pi_x^* & 2cT_{xx} & 2cT_{xy} & 2cT_{xz} \\ \Pi_y^* & 2cT_{xy}^* & 2cT_{yy} & 2cT_{yz} \\ \Pi_z^* & 2cT_{xz}^* & 2cT_{xy}^* & 2cT_{zz} \end{bmatrix}, \tag{3}$$

where $\mathbf{\Theta} = \left[p/\sqrt{\rho_0 c}\ \sqrt{\rho_0 c}\,u_x\ \sqrt{\rho_0 c}\,u_y\ \sqrt{\rho_0 c}\,u_z\right]^{\mathrm{T}}$ is the column vector of acoustic quantities normalized in order to have the same dimensions ($\mathbf{\Theta}^{\mathrm{H}}$ is the Hermitian transpose, i.e. the elements of the transpose matrix are equal to the complex conjugates of the elements of the matrix). The *field matrix* includes components of the complex intensity vector, potential energy density and components of kinetic energy density. The kinetic energy components defined as, for example, $T_{xy} = \rho_0 u_x u_y^*/4$ (with $T_{yx} = T_{xy}{}^*$), can be used to compute the total kinetic energy density $T = T_{xx} + T_{yy} + T_{zz}$ or the curl of the active intensity vector [7]

$$\nabla \times \mathbf{I} = 4\omega\,\mathrm{Im}\{T_{yz}\mathbf{e}_x + T_{zx}\mathbf{e}_y + T_{xy}\mathbf{e}_z\}. \tag{4}$$

The finite-difference approximation is usually employed to approximate a component of the gradient of pressure, then to calculate the particle velocity by using Eq. (2). The pressure between two sensors is expressed by the arithmetic mean of the pressures at the two sensors (finite-sum approximation). By the use of the zero- and first-order terms of the Taylor series expansion

$$p(\mathbf{r}) = \sum_{m=0}^{\infty} \frac{1}{m!}(\mathbf{r}\cdot\nabla)^m p, \tag{5.1}$$

the pressure $p(\mathbf{r})$ at a sensor located at a position $\mathbf{r} = (x, y, z)$ from the origin of the probe is written by

$$p(\mathbf{r}) \approx p + \mathbf{r}\cdot\nabla p, \tag{5.2}$$

where p is the pressure and ∇p is the pressure gradient at the origin of the probe (where the energy quantities are estimated). By taking the example of a probe consisting of 4 microphones (the minimal number of

microphones for a 3D sound intensity probe), Eq. (5.2) is written in the form of a linear system of 4 equations (where $p_i = p(\mathbf{r}_i)$, $i = 1, 2, 3, 4$)

$$\begin{aligned} p_1 &\approx p + x_1\ \partial p/\partial x + y_1\ \partial p/\partial y + z_1\ \partial p/\partial z \\ p_2 &\approx p + x_2\ \partial p/\partial x + y_2\ \partial p/\partial y + z_2\ \partial p/\partial z \\ p_3 &\approx p + x_3\ \partial p/\partial x + y_3\ \partial p/\partial y + z_3\ \partial p/\partial z \\ p_4 &\approx p + x_4\ \partial p/\partial x + y_4\ \partial p/\partial y + z_4\ \partial p/\partial z \end{aligned} \Rightarrow \mathbf{P} \approx \mathbf{M}\,\mathbf{D}, \tag{6}$$

where $\mathbf{P} = [p_1 \quad p_2 \quad p_3 \quad p_4]^{\mathrm{T}}$, $\mathbf{D} = [p \quad \partial p/\partial x \quad \partial p/\partial y \quad \partial p/\partial z]^{\mathrm{T}} = [D_1 \quad D_2 \quad D_3 \quad D_4]^{\mathrm{T}}$ and a matrix $\mathbf{M}$ dependent on the positions of the microphones is given by

$$\mathbf{M} = \begin{bmatrix} 1 & x_1 & y_1 & z_1 \\ 1 & x_2 & y_2 & z_2 \\ 1 & x_3 & y_3 & z_3 \\ 1 & x_4 & y_4 & z_4 \end{bmatrix} = [\,1 \quad \mathbf{x} \quad \mathbf{y} \quad \mathbf{z}\,], \tag{7}$$

To obtain the finite-sum and finite-difference approximation expression for a probe, the approximate values of the vector $\mathbf{D}$ can be written by

$$\mathbf{D} \approx \mathbf{M}^{-1}\mathbf{P}. \tag{8}$$

The inverse of the matrix $\mathbf{M}$ is easily computed by using symbolic computation software [19]. By expressing the coordinates of the 4 microphones with respect to the centre of the probe, the approximate pressure at the central point is $\tilde{p} = D_1$ and the approximations of the three components of the velocity according to the selected system of coordinates are $\tilde{\mathbf{u}} = \mathrm{j}/(\rho_0\omega)[D_2 \ D_3 \ D_4]^{\mathrm{T}}$(the tilde sign $\sim$ over a symbol denotes the approximate value of the corresponding quantity). Substituting the expressions of $\tilde{p}$ and $\tilde{\mathbf{u}}$ into Eq. (1) and then using symbolic computation yield the finite-sum and finite-difference expressions that are usable for experimental measurements. More generally, the column vector of the acoustic quantities $\mathbf{\Theta}$ used for computing the *field matrix* $\mathbf{F}$ (see Eq. (3)) can be written as

$$\mathbf{\Theta} \approx \frac{1}{\sqrt{\rho_0 c}}[D_1 \quad \mathrm{j}D_2/k \quad \mathrm{j}D_3/k \quad \mathrm{j}D_4/k]^{\mathrm{T}}, \tag{9}$$

where $k = \omega/c$ is the wavenumber.

The method described above corresponds to the traditional procedure for measuring the energy quantities of the sound fields by the use of probes consisting of several sensors. The energy quantities in terms of cross-spectral power density are computed by multiplying the pressure and the particle velocity together, which are obtained by the finite-sum and finite-difference approximations. Elko [3] gave an expression for the cross-spectrum between two close microphones as a function of the energy quantities at the central point by using the product of the first terms of the Taylor series of the pressure. By writing similar expressions for each of the microphone pairs of a probe it is possible, from the product of the first three terms of the sum in Eq. (5.1), to obtain a linear system where all the energy quantities of the *field matrix* in Eq. (3) are presented. This development is detailed in Appendix B. Contrary to the method described above, the second-order term of the Taylor series of the pressure is used and, as a result, the approximation of the energy quantities will be a priori more precise. However, it requires the inversion of a linear system of 16 real equations comprising the 16 elementary energy variables, which is not easy to be solved analytically. It is possible, however, to obtain numerical solutions at each frequency. In order to achieve the goal of this article, namely obtaining analytical expressions, the following section is thus devoted to the first approach based on the linear system which is constituted by using the first two terms of the series of Eq. (5.1) and described by Eqs. (6)–(8).

3. Examples of applications

To illustrate the method described in Section 2, examples are given of the computation of the quadratic acoustic quantities for the most widely used 3D-probes consisting of 4–6 microphones. The example of the

6-microphone probe shows how the method based on a linear system of 4 equations can adapt to the redundancy brought by the use of additional microphones. Placing the fifth microphone at the centre of the 4-microphone probe yields a 5-microphone probe that can be used to measure the pressure without approximation. The descriptions of the probes used in this article and the corresponding abbreviations are presented in Appendix A to provide help to the readers. In this section, detail computations are made only on the active intensity and the potential and kinetic energy densities. However, the other acoustic quantities such as the reactive intensity and the curl of active intensity can easily be calculated as well. For the sake of completeness, the calculations of some of these energy quantities are given in Appendix C. In order to make a comparison, the same distance d corresponds to the spacing between 2 microphones placed at the corners of tetrahedron for the probes with 4 and 5 microphones, and to the spacing between 2 microphones placed on the same axis for the probes with 6 microphones (see Fig. 2). In the following computations, the origin of the coordinate system is defined as the geometrical centre of the probe (centroid), $\mathbf{r}_0 = \sum_i^N \mathbf{r}_i/N$. The positions of each microphone are defined from this origin.

3.1. Four-microphone 3D-probes

The 4-microphone probe arrangements are tetrahedral, among which one often finds two types (I and II) shown in Figs. 2(a) and (b). Fig. 1 is the photograph of the type I. This type of probe was exhibited at the *Second International Congress one Acoustic Intensity* in Senlis in 1985 [9] and was studied in Ref. [8]. In Fig. 2(a), the base of the type I tetrahedral probes forming by the microphones 1–3 is parallel to the plane (x, y) and the fourth microphone is located on the positive z-axis. This configuration can be found in the probe described by Suzuki et al. [10], but the axes are different. One can verify, however, that the formulations of these authors can be obtained from Eq. (14) by incrementing the indices by 1 (modulo 4) and by considering that $(I_x, I_y, I_z)_{\text{Suzuki}} = (-I_y, I_z, -I_x)_{\text{type I}}$. For the type II, the 4 microphones are located in two horizontal planes. The first version of this type of probe was proposed by Santos et al. [6]. The 4 microphones are placed on the opposite corners of a cube, whose three orthogonal coordinate axes cross the faces of the cube at their centres. The type II considered here is shown in Fig. (2b), in which the microphones 1 and 2 are aligned in a parallel direction of the x-axis and the microphones 3 and 4 are in a parallel direction of the y-axis. This

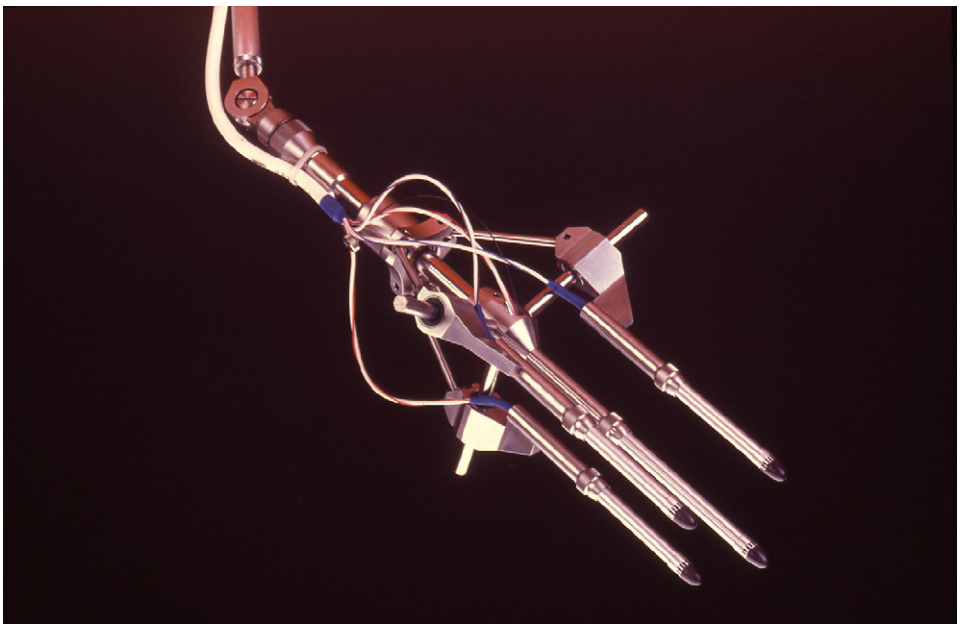

Fig. 1. Tetrahedral probe of the type I with 4 microphones having a base parallel with the (x, y) plane. Model with variable spacing and $\frac{1}{4}$in microphones provided with a cap fixed on their grid to reduce the diffraction effect ([9], photo CETIM).

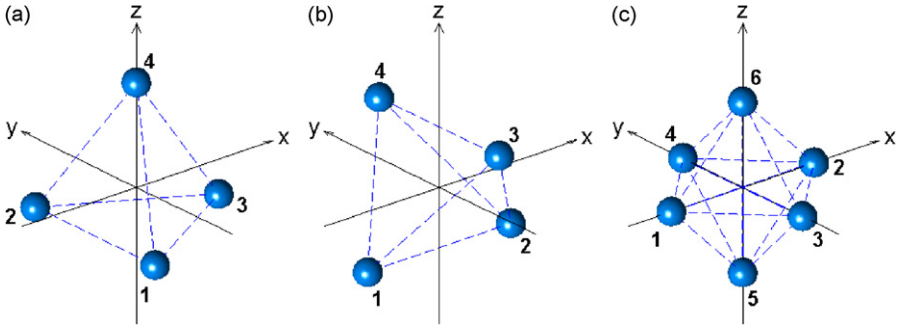

Fig. 2. Microphone configurations for probes studied in this article: (a) tetrahedral probe of the type I with 4 microphones, (b) tetrahedral probe of the type II with 4 microphones, and (c) probe with 6 microphones comprising 3 pairs aligned on the 3 axes.

configuration allows the probe to be more easily oriented in space (a rotation of 45° around the z-axis allows one to find the geometrical arrangement of the probe in Ref. [6]).

One can verify that the centroid is at the probe origin by $[\mathbf{x} \quad \mathbf{y} \quad \mathbf{z}]^{\mathrm{T}} \quad \mathbf{1} = 0$ ($\mathbf{1}$ is, in this case, a column vector with unity for each of the four elements) and the distance from each microphone to the probe centre is $\sqrt{6}d/4$. Using Eq. (7) the matrices $\mathbf{M}$ for the probe types I and II are expressed, respectively, as

$$\mathbf{M}_{\mathrm{I}} = \begin{bmatrix} 1 & -\dfrac{d}{2\sqrt{3}} & -\dfrac{d}{2} & -\dfrac{d}{2\sqrt{6}} \\ 1 & -\dfrac{d}{2\sqrt{3}} & \dfrac{d}{2} & -\dfrac{d}{2\sqrt{6}} \\ 1 & \dfrac{d}{\sqrt{3}} & 0 & -\dfrac{d}{2\sqrt{6}} \\ 1 & 0 & 0 & \dfrac{\sqrt{6}d}{4} \end{bmatrix} \quad \text{and} \quad \mathbf{M}_{\mathrm{II}} = \begin{bmatrix} 1 & -\dfrac{d}{2} & 0 & -\dfrac{d}{2\sqrt{2}} \\ 1 & \dfrac{d}{2} & 0 & -\dfrac{d}{2\sqrt{2}} \\ 1 & 0 & -\dfrac{d}{2} & \dfrac{d}{2\sqrt{2}} \\ 1 & 0 & \dfrac{d}{2} & \dfrac{d}{2\sqrt{2}} \end{bmatrix}. \tag{10}$$

The finite-sum and finite-difference approximate expressions of the vector $\mathbf{D}$ for type I and II are, respectively, obtained from symbolic calculation using Eq. (8)

$$\mathbf{D}_{\mathrm{I}} = \begin{bmatrix} p \\ \partial p/\partial x \\ \partial p/\partial y \\ \partial p/\partial z \end{bmatrix} \approx \begin{bmatrix} (p_1+p_2+p_3+p_4)/4 \\ (2p_3-p_1-p_2)/(\sqrt{3}d) \\ (p_2-p_1)/d \\ (3p_4-p_1-p_2-p_3)/(\sqrt{6}d) \end{bmatrix}, \quad \mathbf{D}_{\mathrm{II}} = \begin{bmatrix} p \\ \partial p/\partial x \\ \partial p/\partial y \\ \partial p/\partial z \end{bmatrix} \approx \begin{bmatrix} (p_1+p_2+p_3+p_4)/4 \\ (p_2-p_1)/d \\ (p_4-p_3)/d \\ (p_4+p_3-p_1-p_2)/(\sqrt{2}d) \end{bmatrix}. \tag{11}$$

Eq. (11) is used for computation of the column vector of the acoustic quantities $\mathbf{\Theta}$ by which the finite-difference and -sum approximation of the field matrix is obtained by Eq. (3). It thus seems that each element F_{mn} of the field matrix is a linear combination of the cross-products $\frac{1}{2}p_i^* p_j$. The 3 components of the active intensity and the potential and kinetic energy densities are then obtained by

$$\tilde{I}_x = \mathrm{Re}\{\tilde{F}_{12}\}, \quad \tilde{I}_y = \mathrm{Re}\{\tilde{F}_{13}\}, \quad \tilde{I}_z = \mathrm{Re}\{\tilde{F}_{14}\}, \quad \tilde{V} = \frac{\tilde{F}_{11}}{2c} \quad \text{and} \quad \tilde{T} = \frac{1}{2c}\sum_{m=2}^{4} \tilde{F}_{mm}. \tag{12}$$

For practical applications, these quantities should be written in the form of one-sided cross-spectral densities by using the following notation [11]:

$$G_{ij}(\omega) = C_{ij}(\omega) + \mathrm{j}Q_{ij}(\omega) = \lim_{T\to\infty} \frac{2}{T} E[P_i^*(\omega, T)P_j(\omega, T)], \tag{13}$$

which corresponds formally to the terms of the complex notation $\frac{1}{2}p_i^* p_j$. $P_i(\omega, T)$ is the Fourier transform of the ith microphone signal over a finite length T. The expressions for the intensity and the acoustic energy densities obtained by using Eqs. (12)–(13) for the probes type I and II are, respectively, given by the following (see Appendix A):

Probe type I (4MI)

$$\begin{aligned}
\tilde{I}_x(\omega) &= \frac{1}{4\sqrt{3}\rho_0 ckd}[3Q_{31}(\omega) + 3Q_{32}(\omega) + Q_{41}(\omega) + Q_{42}(\omega) - 2Q_{43}(\omega)],\\
\tilde{I}_y(\omega) &= \frac{1}{4\rho_0 ckd}[2Q_{21}(\omega) + Q_{31}(\omega) + Q_{41}(\omega) - Q_{32}(\omega) - Q_{42}(\omega)],\\
\tilde{I}_z(\omega) &= \frac{1}{\sqrt{6}\rho_0 ckd}[Q_{41}(\omega) + Q_{42}(\omega) + Q_{43}(\omega)],
\end{aligned} \tag{14}$$

$$\tilde{V}(\omega) = \frac{1}{2(4^2)\rho_0 c^2}\sum_{i=1}^{4}\sum_{j=1}^{4} G_{ij}(\omega) = \frac{1}{2(4^2)\rho_0 c^2}\sum_{i=1}^{4} G_{ii}(\omega) + \frac{1}{(4^2)\rho_0 c^2}\sum_{i=2}^{4}\sum_{j=1}^{i-1} C_{ij}(\omega), \tag{15}$$

$$\tilde{T}(\omega) = \frac{3}{4\rho_0 c^2 k^2 d^2}\sum_{i=1}^{4} G_{ii}(\omega) - \frac{1}{2\rho_0 c^2 k^2 d^2}\sum_{i=2}^{4}\sum_{j=1}^{i-1} C_{ij}(\omega). \tag{16}$$

Probe type II (4MII)

$$\begin{aligned}
\tilde{I}_x(\omega) &= \frac{1}{4\rho_0 ckd}[2Q_{21}(\omega) + Q_{31}(\omega) + Q_{41}(\omega) - Q_{32}(\omega) - Q_{42}(\omega)],\\
\tilde{I}_y(\omega) &= \frac{1}{4\rho_0 ckd}[Q_{41}(\omega) + Q_{42}(\omega) + 2Q_{43}(\omega) - Q_{31}(\omega) - Q_{32}(\omega)],\\
\tilde{I}_z(\omega) &= \frac{1}{2\sqrt{2}\rho_0 ckd}[Q_{41}(\omega) + Q_{42}(\omega) + Q_{31}(\omega) + Q_{32}(\omega)].
\end{aligned} \tag{17}$$

The approximate expression for the potential energy density for the type II is the same as that for the type I Eq. (15), because both have the same approximate expression for the sound pressure. It is also the case for the kinetic energy density, although the finite-difference and finite-sum approximations of the components of the particle velocity are different between the two types (see Eq. (11)).

3.2. Five-microphone 3D-probes

The approximation of the pressure at the central point between 2 microphones estimated from the arithmetic mean of their pressures is less accurate than that estimated from the gradient of pressure using the finite-difference approximation, as shown by the following equations [12–14]:

$$\frac{p_2 + p_1}{2} = p\cos(kd\cos\alpha/2), \quad \frac{p_2 - p_1}{d} = \frac{\partial p}{\partial r}\frac{\sin(kd\cos\alpha/2)}{kd\cos\alpha/2}, \tag{18}$$

where α is the angle of the direction for an incident plane wave with respect to the r-axis of the 2 microphones and d is the microphone spacing. In order to improve the accuracy, the fifth microphone is placed at the centre of the 4-microphone probe. To obtain the expressions of energy quantities, one just needs to replace the arithmetic mean of the pressure in the first element of the vector **D** in Eq. (11) by p_5

$$D_1 = p_5, \tag{19}$$

and to compute again the *field matrix* **F**. Using Eq. (12) yields the new expressions of the components of the active intensity for the two types of probes:

Probe type I (5MI)

$$\tilde{I}_x(\omega) = \frac{1}{\sqrt{3}\rho_0 ckd}[Q_{51}(\omega) + Q_{52}(\omega) - 2Q_{53}(\omega)],$$
$$\tilde{I}_y(\omega) = \frac{1}{\rho_0 ckd}[Q_{51}(\omega) - Q_{52}(\omega)],$$
$$\tilde{I}_z(\omega) = \frac{1}{\sqrt{6}\rho_0 ckd}[Q_{51}(\omega) + Q_{52}(\omega) + Q_{53}(\omega) - 3Q_{54}(\omega)]. \tag{20}$$

Probe type II (5MII)

$$\tilde{I}_x(\omega) = \frac{1}{\rho_0 ckd}[Q_{51}(\omega) - Q_{52}(\omega)],$$
$$\tilde{I}_y(\omega) = \frac{1}{\rho_0 ckd}[Q_{53}(\omega) - Q_{54}(\omega)],$$
$$\tilde{I}_z(\omega) = \frac{1}{\sqrt{2}\rho_0 ckd}[Q_{51}(\omega) + Q_{52}(\omega) - Q_{53}(\omega) - Q_{54}(\omega)]. \tag{21}$$

The expression for the kinetic energy density for the two types of the 5-microphone probes is the same as that for the 4-microphone probes (see Eq. (16)). The potential energy density for both types of 5-microphone probes is given by

$$\tilde{V}(\omega) = \frac{G_{55}(\omega)}{2\rho_0 c^2}. \tag{22}$$

3.3. Six-microphone 3D-probes

The 6 microphones in the probe are aligned two by two along the x, y and z axes [15] (Fig. 2c) with a spacing of d. Applying the above method yields a matrix **M** of 6×4 size which produces an over-determined system. This shows well that using a 6-microphone probe results in redundant information. To calculate the inverse of the matrix **M** in the system of equations given by Eq. (6) for this configuration, one should consider the pseudo-inversion $(\mathbf{M}^{\mathrm{T}}\mathbf{M})^{-1}\mathbf{M}^{\mathrm{T}}$. Applying the symbolic calculation, the approximate expression for the vector **D** is obtained

$$\mathbf{D} = \begin{bmatrix} p \\ \partial p/\partial x \\ \partial p/\partial y \\ \partial p/\partial z \end{bmatrix} \approx \begin{bmatrix} (p_1 + p_2 + p_3 + p_4 + p_5 + p_6)/6 \\ (p_2 - p_1)/d \\ (p_4 - p_3)/d \\ (p_6 - p_5)/d \end{bmatrix}. \tag{23}$$

Pressure obtained by the approximation $p \approx D_1$ is the arithmetic mean of the 6-microphone pressures (probe 6MAV, AV: average). Thus, the approximation of the pressure together with the finite-difference approximation of the particle velocity leads to computing 15 cross-spectra between the 6 microphones, which are used to compute the energy quantities by Eq. (12). The field matrix for the 6-microphone probe can be obtained by taking Eq. (23) into account and using Eqs. (3) and (9). The approximations for the three

components of the active intensity are given by

$$\tilde{I}_x(\omega)=\frac{1}{6\rho_0 ckd}\sum_{i=1}^{6}\mathrm{Im}\{G_{i1}(\omega)-G_{i2}(\omega)\}=\frac{1}{6\rho_0 ckd}\left[2Q_{21}(\omega)+\sum_{i=3,4,5,6}\left(Q_{i1}(\omega)-Q_{i2}(\omega)\right)\right],$$

$$\tilde{I}_y(\omega)=\frac{1}{6\rho_0 ckd}\sum_{i=1}^{6}\mathrm{Im}\{G_{i3}(\omega)-G_{i4}(\omega)\}=\frac{1}{6\rho_0 ckd}\left[2Q_{43}(\omega)+\sum_{i=1,2,5,6}\left(Q_{i3}(\omega)-Q_{i4}(\omega)\right)\right],$$

$$\tilde{I}_z(\omega)=\frac{1}{6\rho_0 ckd}\sum_{i=1}^{6}\mathrm{Im}\{G_{i5}(\omega)-G_{i6}(\omega)\}=\frac{1}{6\rho_0 ckd}\left[2Q_{65}(\omega)+\sum_{i=1,2,3,4}\left(Q_{i5}(\omega)-Q_{i6}(\omega)\right)\right]. \quad (24)$$

It is noted that the expression for each component comprises 9 cross-spectral densities. The approximation for the potential energy density proportional to the sum of all the elements of the cross-spectral matrix of the 6-microphone signals is expressed by

$$\tilde{V}(\omega)=\frac{1}{2(6^2)\rho_0 c^2}\sum_{i=1}^{6}\sum_{j=1}^{6}G_{ij}(\omega)=\frac{1}{2(6^2)\rho_0 c^2}\sum_{i=1}^{6}G_{ii}(\omega)+\frac{1}{(6^2)\rho_0 c^2}\sum_{i=2}^{6}\sum_{j=1}^{i-1}C_{ij}(\omega), \quad (25)$$

and the kinetic energy density is given by

$$\tilde{T}(\omega)=\frac{1}{2\rho_0 c^2k^2d^2}\sum_{i=1}^{6}G_{ii}(\omega)-\frac{1}{\rho_0 c^2k^2d^2}[C_{21}(\omega)+C_{43}(\omega)+C_{65}(\omega)]. \quad (26)$$

However the above approach has, to our knowledge, rarely been used for the 6-microphone probe. The solution often adopted is to use the redundancy of information to simplify the formulation for the measurements [15]. The idea is to consider the 2 microphones along each axis as a single 1D probe. The approximations for the pressure and the gradient of pressure at the mid-point of the 2 microphones are estimated, respectively, from the arithmetic mean of their pressures and by using the finite-difference approximation. To adapt this configuration to our computational method, the linear system will be constructed by considering $p_{1,2}\approx p_x\mp(d/2)\partial p/\partial x$, $p_{3,4}\approx p_y\mp(d/2)\partial p/\partial y$, $p_{5,6}\approx p_z\mp(d/2)\partial p/\partial z$, where p_x, p_y and p_z are, respectively, approximations of the pressures for 1D probe on the three axes. This system results in a 6×6 matrix $\mathbf{M}$. The inverse of $\mathbf{M}$ will give approximate values for the vector $\mathbf{D}=[p_x\quad p_y\quad p_z\quad \partial p/\partial x\quad \partial p/\partial y\quad \partial p/\partial z]^{\mathrm{T}}$, in which $p_x\approx(p_1+p_2)/2$, $p_y\approx(p_3+p_4)/2$ and $p_z\approx(p_5+p_6)/2$, whereas the approximations for $\partial p/\partial x$, $\partial p/\partial y$ and $\partial p/\partial z$ are the same as those in Eq. (23). A modified vector of 6 elements $\mathbf{\Theta}'=\left[p_x/\sqrt{\rho_0 c}\ \ p_x/\sqrt{\rho_0 c}\ \ p_z/\sqrt{\rho_0 c}\ \ \sqrt{\rho_0 c}u_x\ \ \sqrt{\rho_0 c}u_y\ \ \sqrt{\rho_0 c}u_z\right]^{\mathrm{T}}$ is constituted from the vector $\mathbf{D}$ and written as

$$\mathbf{\Theta}'\approx\left(1/\sqrt{\rho_0 c}\right)[D_1\quad D_2\quad D_3\quad \mathrm{j}D_4/k\quad \mathrm{j}D_5/k\quad \mathrm{j}D_6/k]^{\mathrm{T}}. \quad (27)$$

The intermediate 6-by-6 matrix can be obtained by using $\mathbf{\Phi}'=\frac{1}{2}\mathbf{\Theta}'\mathbf{\Theta}'^{\mathrm{H}}$, which allows the field matrix to be reconstituted from its elements in the following way:

$$\mathbf{F}\approx\begin{bmatrix}\frac{1}{3}\left(\Phi'_{11}+\Phi'_{22}+\Phi'_{33}\right) & \Phi'_{14} & \Phi'_{25} & \Phi'_{36}\\ \Phi'_{41} & \Phi'_{44} & \Phi'_{45} & \Phi'_{46}\\ \Phi'_{52} & \Phi'_{54} & \Phi'_{55} & \Phi'_{56}\\ \Phi'_{63} & \Phi'_{64} & \Phi'_{65} & \Phi'_{66}\end{bmatrix}. \quad (28)$$

By using Eq. (12), the three components of the active acoustic intensity for this probe (6M3A, 3A: three axis) are then given as follows:

$$\tilde{I}_x(\omega)=\frac{Q_{21}(\omega)}{\rho_0 ckd},\quad \tilde{I}_y(\omega)=\frac{Q_{43}(\omega)}{\rho_0 ckd},\quad \tilde{I}_z(\omega)=\frac{Q_{65}(\omega)}{\rho_0 ckd}, \quad (29)$$

and the potential energy density is

$$\tilde{V}(\omega) = \frac{1}{24\rho_0 c^2}\sum_{i=1}^{6} G_{ii}(\omega) + \frac{1}{12\rho_0 c^2}[C_{21}(\omega) + C_{43}(\omega) + C_{65}(\omega)]. \tag{30}$$

The kinetic energy density is, of course, identical to that of the preceding probe (see Eq. (26)).

For the probes with 7 microphones, Cazzolato and Hansen [4] added a seventh microphone to the probe, leading to improved performance. They are not included here because this solution presents the disadvantage of imposing heavy constraints in its practical realization, which causes it never to be used in practice.

4. Comparisons of probe performance

In the absence of all other instrumentation errors, the errors caused by the finite-difference and sum approximation technique are significant mainly at high frequencies. The proximity of point sources can bring additional errors due to the sphericity of the wave front, which increase with the directivity and the order of the sources [12,13]. From the study of 1D probes, it has been concluded that the distance from the monopole, dipole or quadrupole sources to the probe centre must be greater than $2d$ in order that the error in the intensity is lower than 1 dB (d is the microphone spacing). In practice, for extended surfaces the low-limit distance can be reduced to the microphone spacing d. Experiences show that the use of plane waves with different angles of incidence allows one to evaluate the magnitude of these errors at high frequencies and to define the limit for the use of probes. Therefore, in this section the intensity vector and energy density are calculated for plane waves as a function of the angle of incidence. For the plane waves we define the angle of incidence as (θ, ϕ), where θ and ϕ are, respectively, azimuth and elevation angles, see Fig. (4a). The magnitude of the active intensity is written by $I_0 = A^2/(2\rho_0 c)$, with A the amplitude of the plane wave. The pressure is expressed as

$$p(x,y,z) = A\mathrm{e}^{-\mathrm{j}kr} = A\,\exp(-\mathrm{j}kx\,\cos\,\theta\,\cos\,\phi - \mathrm{j}ky\,\cos\,\theta\,\sin\,\phi - \mathrm{j}kz\,\sin\,\theta). \tag{31}$$

where

$$\mathbf{k} = (k\,\cos\,\theta\,\cos\,\phi, k\,\cos\,\theta\,\sin\,\phi, k\,\sin\,\theta), \tag{32}$$

is the wavenumber vector and $\mathbf{r} = (x, y, z)$ is the coordinates with respect to the centre of the probe (Fig. 4a). The errors are also obtained by symbolic computation. The maximum and minimum values of the errors are numerically evaluated. The results are shown in Figs. 3–9.

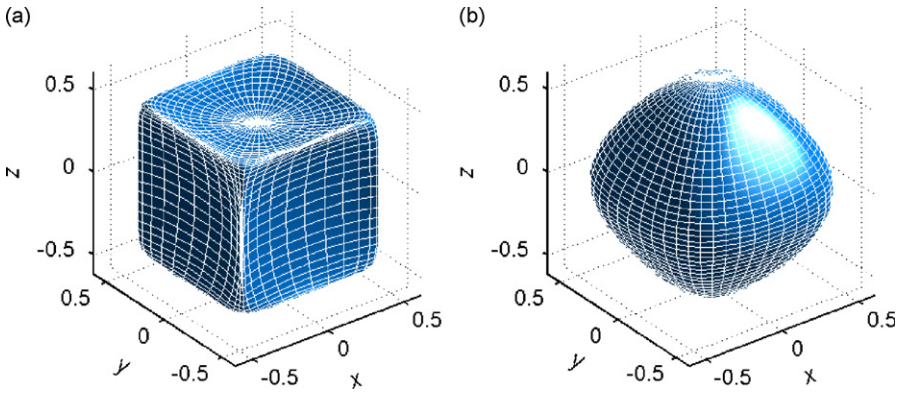

Fig. 3. Illustration of the fluctuations of the estimated values of the amplitude of the active intensity vector at $kd = 2.2$ corresponding to a unit intensity vector produced by a plane wave coming in all directions: (a) for the probe with 6 microphones (6M3A) and (b) for the probe with 4 microphones (4MI).

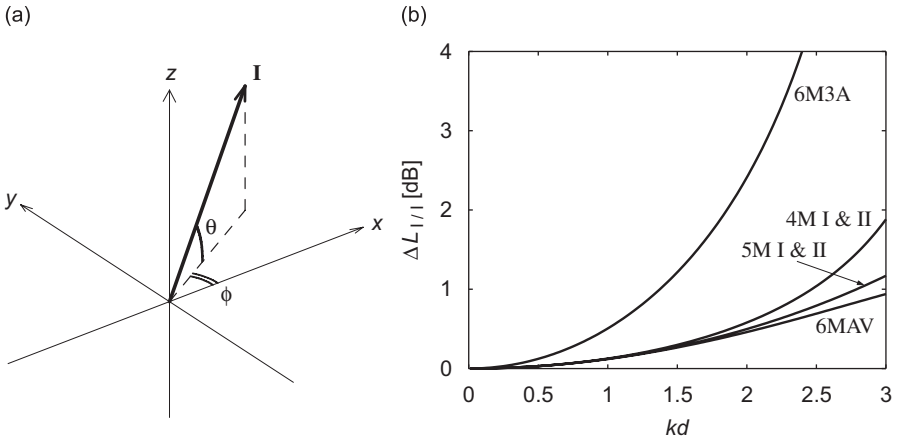

Fig. 4. (a) Notation used for the incident plane wave and (b) intervals of variation $\Delta L_{|\mathbf{I}|}$ of the estimate of the modulus of the intensity vector versus kd for the six probes.

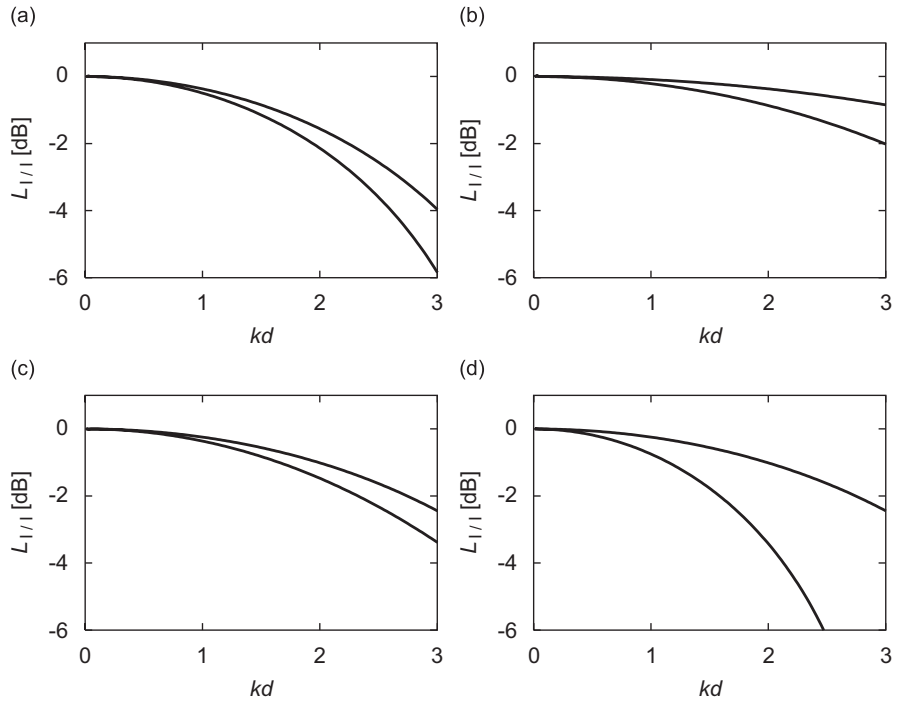

Fig. 5. Extreme bounds for variation of the modulus of the active intensity vector versus kd when the angle of incidence of the progressive plane wave varies: (a) 4-microphone probes of the types I and II, (b) 5-microphone probes of the types I and II, (c) 6-microphone probe with averaged pressure (6MAV) and (d) 6-microphone probe processed as 3 one-dimensional probes (6M3A).

4.1. Errors in the estimate of the magnitude of the active intensity

In comparison to the 1D probes, the 3D probes have some characteristics that can easily be made obvious by considering the estimate of both the magnitude and direction of the intensity vector of the 6-microphones probe (6M3A: the three axes are treated separately). Expressing pressure at each microphone by Eq. (31) and then calculating the magnitude of the active intensity vector $|\tilde{\mathbf{I}}| = \sqrt{\tilde{I}_x^2 + \tilde{I}_y^2 + \tilde{I}_z^2}$ by Eq. (29) yields the

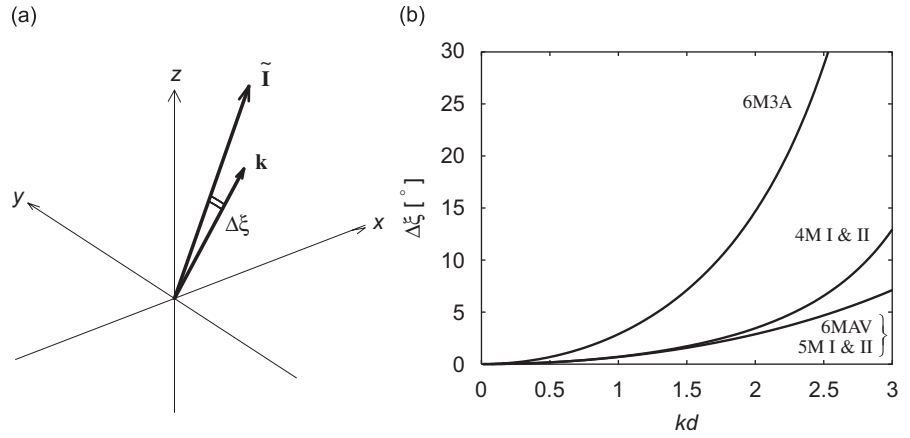

Fig. 6. (a) Error in the orientation angle of the estimated vector $\tilde{\mathbf{I}}$ and (b) Maximum values in degrees of this error as a function of kd for the various probes.

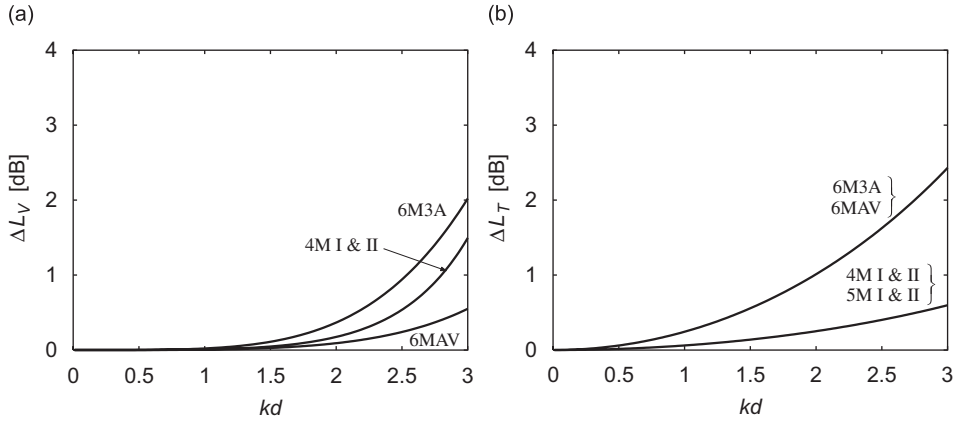

Fig. 7. Bounds for the energy density estimates versus kd for the five probes: (a) bounds of variation for the potential energy density ΔL_V and (b) bounds of variation for the energy kinetic density ΔL_T.

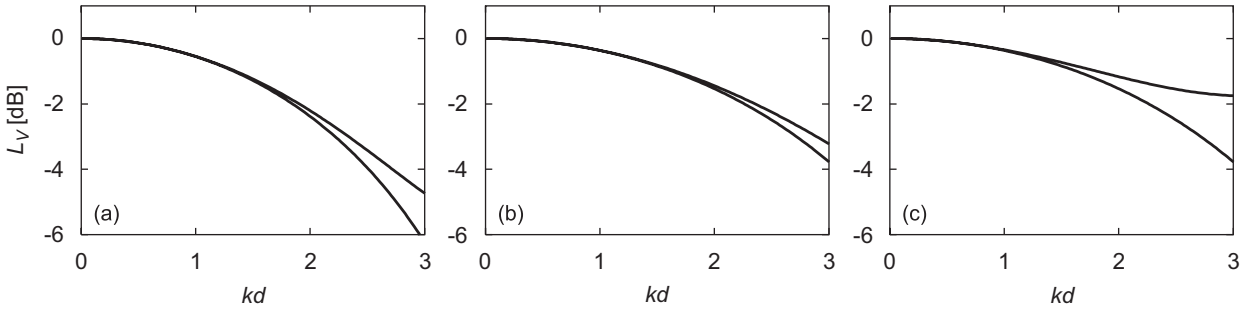

Fig. 8. Extreme bounds of variation of the potential energy density versus kd when the angle of incidence of the progressive plane wave varies: (a) 4-microphone probes of the type I and II, (b) 6-microphone probe with averaged pressure (6MAV) and (c) 6-microphone probe used as independent pairs (6M3A).

expression for the relative error in estimating the magnitude of active intensity:

$$\frac{|\tilde{\mathbf{I}}(\omega)|}{I_0} = 1 + \varepsilon_{|\mathbf{I}|} = \frac{\sqrt{\sin^2(kd\cos\theta\cos\phi) + \sin^2(kd\cos\theta\sin\phi) + \sin^2(kd\sin\theta)}}{kd}. \tag{33}$$

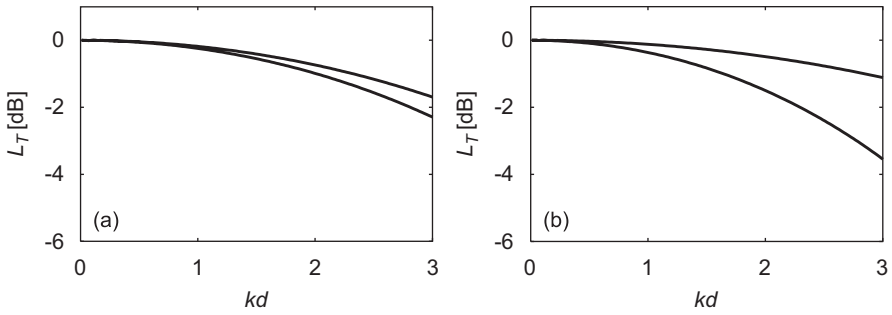

Fig. 9. Extreme bounds of variation of the kinetic energy density versus kd when the angle of incidence of the progressive plane wave varies: (a) probes with 4 and 5 microphones of the type I and II and (b) 6-microphone probes with averaged pressure (6MAV) and used as independent pairs (6M3A).

Eq. (33) shows that the error in estimating of the magnitude of the active intensity is dependent of the angles of incidence (θ, ϕ) as well on kd. When the value of kd increases, the estimate of the intensity magnitude is always lower than its true value, as is shown in Fig. 3a for a unit intensity vector in all directions when $kd = 2.2$. If sound wave propagates in the direction of axis of a pair of microphones, one can obtain the maximum error of the 1D probes [16]. For example, for $\theta = 0$ and $\phi = 0$, the error is maximum and represents the lower bound

$$\left.\frac{|\tilde{\mathbf{I}}(\omega)|}{I_0}\right|_{\text{inf}} = \frac{|\tilde{I}_x(\omega)|}{I_0} = \frac{\sin\, kd}{kd}. \tag{34}$$

On the contrary, the error will be minimum when the apparent spacing of microphone in the direction of wave propagation is the smallest [16]. For the probe shown in Fig. 2c, this condition is satisfied when the incidence angle with respect to each axis is identical, i.e. when the three components of the active intensity have identical absolute values. In this case ($\theta = \pm \arcsin 1/\sqrt{3}$, $\phi = \pm\pi/4 \pm \pi/2$), we obtain a high bound of uncertainty

$$\left.\frac{|\tilde{\mathbf{I}}(\omega)|}{I_0}\right|_{\text{sup}} = \frac{\sin\left(kd/\sqrt{3}\right)}{kd/\sqrt{3}}. \tag{35}$$

The magnitude of the estimated intensity vector fluctuates between these two bounds according to the incidence angles (θ, ϕ) of the plane waves. This error, that depends at the same time on kd and on the direction of the wave propagation (θ, ϕ), can be corrected for a plane wave incident at a single angle. Unfortunately, the estimated direction will often be that of a resulting vector of the contribution from waves coming from different directions and the correction is not possible. Thus, it has, in practice, to tolerate an uncertainty limited by the bounds defined by Eqs. (34) and (35) for the probe 6M3A. For the other probes, the expressions obtained by the symbolic computation are much more complicated. The estimates of the magnitude of a unit intensity vector are shown in Fig. 3b for the probe 4MI at $kd = 2.2$. In Fig. 4b are shown the comparisons of the difference between the high and low bounds $\Delta L_{|\mathbf{I}|} = L_{|\mathbf{I}|}\big|_{\text{sup}} - L_{|\mathbf{I}|}\big|_{\text{inf}}$ for the probes consisting, respectively, 4, 5 and 6 microphones. The two bounds $L_{|\mathbf{I}|}\big|_{\text{sup}}$ and $L_{|\mathbf{I}|}\big|_{\text{inf}}$ of each of these probes are, respectively, illustrated in Figs. 5a–d.

4.2. Error in the estimate of the direction of the active intensity vector

By considering the 3D probe, similar kinds of remarks as those in the above sub-section can be made. The error in the estimate of the direction of the active intensity for the 6M3A probe is zero (i) when the plane wave propagates along the direction of an axis of a pair of microphones, (ii) when one component is zero and the two others have identical absolute values or (iii) when the absolute values of the three components are identical. Otherwise, the error in the estimate of the direction of the active intensity increases with kd. This

error corresponds to the angle formed by the wave vector $\mathbf{k}$ and the estimated intensity vector $\tilde{\mathbf{I}}$ (Fig. 6a) and is expressed as

$$\Delta\xi = \arccos\frac{\mathbf{k}\cdot\tilde{\mathbf{I}}}{k|\tilde{\mathbf{I}}|}. \tag{36}$$

The maximum value of the error $\Delta\xi$ (in degree) is shown in Fig. 6(b) for the six probes.

4.3. Errors in the estimate of the energy densities

An evaluation similar to that for the magnitude of the intensity vector is made for the estimate of the potential energy density $\tilde{V}$ and kinetic energy density $\tilde{T}$, which is expressed in terms of kd and the direction of the wave propagation (θ, ϕ). The ratio of $4\rho_0c^2\tilde{V}/A^2$ to $4\rho_0c^2\tilde{T}/A^2$ is calculated in the function of θ and ϕ. For each value of kd, the maximum and minimum errors provide, respectively, the lower and upper bounds. The differences between the upper and lower bounds ΔL_V and ΔL_T (both in dB) are shown in Fig. 7 for the different type of probes. Figs. 8 and 9 show the bounds of this error versus kd for each of the six probes. The 5-microphone probe, for which the pressure is measured by the microphone at the probe centre, can be used to estimate the potential energy density without bias. In addition, the fact that the type I and type II of the 4- and 5-microphone probes have the same approximate expressions for the pressure gradient leads to the same estimations of the kinetic energy density, just like the two types of 6-microphone probes.

4.4. Comments

4.4.1. High limit of the frequency range

From the above analysis on the behaviour of the probes for an incident plane wave, the inherent error caused by the finite-difference and sum approximation depends on the travelling wave direction and on the non-dimensional parameter of frequency kd. The high-frequency limit for using each probe can be obtained by fixing a criterion for the maximum error. The error to be considered is the difference between the upper and lower bounds, because a correction by the average values of the upper and lower bound curves can be made in calculating the magnitude of the active intensity. As in the measurements of 3D intensity, the estimate of the direction of a vector is of primary importance; it is a criterion limiting the uncertainty on $\Delta\xi$ that is selected here to compare the probes. By inspection of the curves $\Delta\xi$ versus kd shown in Fig. 6, the high-frequency limit for use of the probes is obtained by determining k_Ld at a maximum uncertainty $\Delta\xi = 5^\circ$. Table 1 contains the values k_Ld for each probe. The maximum errors of the magnitude of the intensity $\Delta L_{|\mathbf{I}|}$ and the potential and kinetic energy densities ΔL_V, ΔL_T are also given in Table 1.

4.4.2. Other four-microphones probes

The tetrahedral disposition of the microphones is not found in one of the first 3D probes used for the experimental characterization of acoustic intensity fields described by Vandenhout et al. [17] and then named "cubic probe" by Cazzolato and Ghan [5] in their work. The first microphone is placed at the origin of an orthogonal coordinate system, the other 3 microphones are, respectively, placed on each axes with a distance d from the origin. The x-component of the intensity is estimated by a microphone pair (1–2), the y-component by the microphone pair (1–3) and the z-component by the microphone pair (1–4). The authors mentioned in

Table 1
Comparison of the performance of the probes for a progressive one-dimensional plane wave

Probe	k_Ld for $\Delta\xi = 5^\circ$	$\Delta L_{\|\mathbf{I}\|}$ (dB)	ΔL_V (dB)	ΔL_T (dB)
4M types I and II	2.294	0.82	0.34	0.33
5M types I and II	2.588	0.85	0	0.43
6M AV	2.575	0.73	0.27	1.73
6M 3A	1.287	0.87	0.06	0.41

[17] that "the resulting intensity components consequently do not relate to one single point, but only approximate the intensity components for that point". However, by considering the microphone 1 as the centre of the probe where the energy quantities will be estimated (probe 4MV), the use of the procedure described by Eqs. (7)–(9), (3) and (12) leads to the formulations in Ref. [17] for the vector **D** and the three components of the active intensity

$$\mathbf{D} \approx \begin{bmatrix} p_1 & (p_2 - p_1)/d & (p_3 - p_1)/d & (p_4 - p_1)/d \end{bmatrix}^{\mathrm{T}}, \tag{37}$$

$$\tilde{I}_x(\omega) = \frac{Q_{21}(\omega)}{\rho_0 ckd}, \quad \tilde{I}_y(\omega) = \frac{Q_{31}(\omega)}{\rho_0 ckd}, \quad \tilde{I}_z(\omega) = \frac{Q_{41}(\omega)}{\rho_0 ckd}. \tag{38}$$

The potential energy density is naturally expressed as a function of the auto-spectrum of only microphone 1 and the kinetic energy is expressed by

$$\tilde{T}(\omega) = \frac{1}{2\rho_0 c^2 k^2 d^2} \left[3G_{11}(\omega) + \sum_{i=2}^{4} 2C_{i1}(\omega) - G_{ii}(\omega) \right]. \tag{39}$$

Another approach can be chosen by calculating the energy quantities at the geometrical centre (the centroid) of the probe, the position of which in the coordinates of probe 4MV is $\mathbf{r}_0 = \sum_{i=1}^{4} \mathbf{r}_i/4 = [d/4 \quad d/4 \quad d/4]^{\mathrm{T}}$. The following equation is thus obtained (probe 4MC):

$$\mathbf{D} \approx \begin{bmatrix} (p_1 + p_2 + p_3 + p_4)/4 & (p_2 - p_1)/d & (p_3 - p_1)/d & (p_4 - p_1)/d \end{bmatrix}^{\mathrm{T}}, \tag{40}$$

$$\tilde{I}_\mu(\omega) = \frac{1}{4\rho_0 ckd} \left(2Q_{ii}(\omega) + \sum_{\substack{j=1 \\ j \neq i}}^{4} Q_{j1}(\omega) - Q_{ji}(\omega) \right) \quad \text{for} \quad \begin{cases} \mu = x, & i = 1, \\ \mu = y, & i = 2, \\ \mu = z, & i = 3, \end{cases} \tag{41}$$

$$\tilde{V}(\omega) = \frac{1}{32\rho_0 c^2} \left(\sum_{i=1}^{6} G_{ii}(\omega) + \sum_{i=1}^{3} \sum_{j=i+1}^{4} C_{ij}(\omega) \right). \tag{42}$$

The kinetic energy density is also expressed by Eq. (39). For the two probes, Fig. 10 shows the bounds of variation of these different quantities when the angle of incidence of the progressive plane wave Eq. (39) varies with respect to the probes. It is noticed that the two probes have identical performances for the kinetic energy density (due to the same formulation). It is also shown that probe 4 MV, the microphone 1 of which is at the origin, does not show an error in the measurement of the potential energy density and presents better results for the active intensity—completely similar to the probe 6MA comprising 6 microphones (Figs. 5–9).

4.4.3. Behaviour of probes in more complicated fields

The results presented in this paper correspond to the most elementary sound field: the plane progressive wave. The studies of the 1D probe for the acoustic intensity have shown that this simple field could sufficiently provide a realistic estimate of the errors and the high-frequency limit of the use of the probes. If a quasi-stationary wave is considered,

$$p(\mathbf{r}) = A \left| \mathrm{e}^{-j\mathbf{k}\cdot\mathbf{r}} + R\mathrm{e}^{j\phi}\mathrm{e}^{j\mathbf{k}\cdot\mathbf{r}} \right|, \tag{43}$$

it is possible to note that the results concerning the bias error of the acoustic intensity (magnitude and orientation angle of the vector), shown in Figs. 3–6 and 10a–b, do not change with the values of the reflection coefficient R. One can also note that these results are independent of the position of the probe with respect to the maximum and minimum values of the pressure ($0 \leq \phi \leq \pi$). Unfortunately, it is not the case for the bias error of the potential and kinetic energy densities. Cazzolato and Hansen [4] have already observed different errors in progressive and stationary waves from the studies on the estimated values of the total energy density.

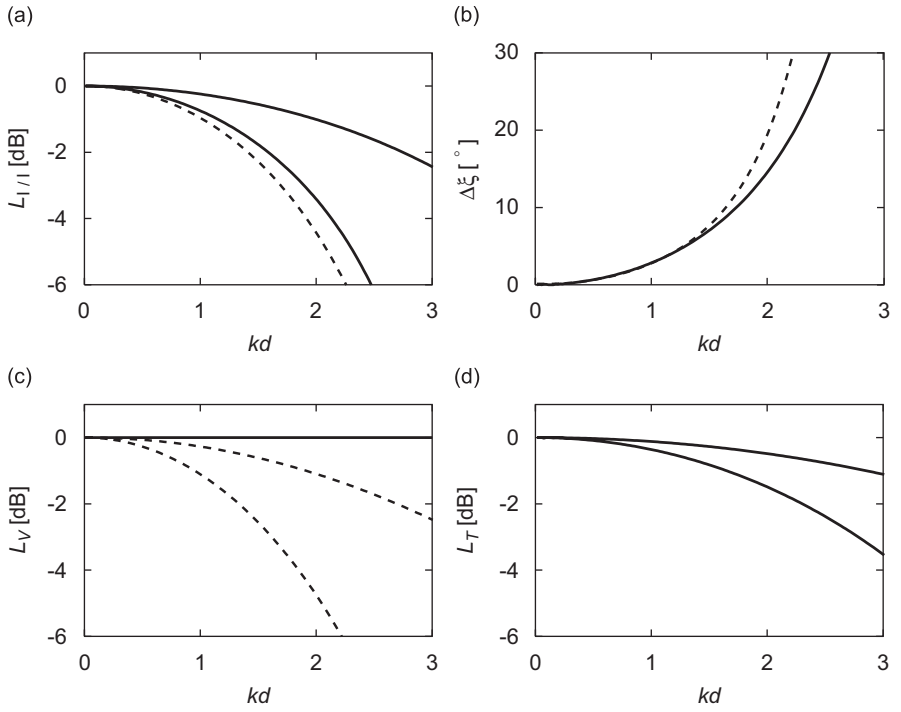

Fig. 10. Extreme bounds of variation when the angle of incidence of the progressive plane wave varies for the probes 4MV and 4MC: (a) modulus of the active intensity vector, (b) orientation angle of the estimated active intensity vector, (c) potential energy density and (d) kinetic energy density.

When $R = 1$, these errors are maxima. Fig. 11 illustrates the errors in $\tilde{T}$, $\tilde{V}$ and $\tilde{E}$ versus the position of the centre of the 4 microphone probe of type I (4MI) in the standing wave for $kd = 1$ and for the limit values $k_L d = 2.3$.

4.4.4. Synthesis

There are no differences in performance between the tetrahedral probes of types I and II. The orientation of the probe does not have an influence on the magnitude of the errors. Though the formulae for the active intensity written in terms of the cross-spectral power densities are different for the two types of probes, they lead to inherent errors with the same magnitude. By using our method for the configuration of the tetrahedral probe of Santos et al. [6] the same formulations are obtained as those presented in their publication, but the performance obtained are the same as those of types I and II. Adding the fifth microphone at the centre of the 4-microphone probe brings a limited improvement by increasing 13% the high-frequency limit. In counterpart, the smallest distance between 2 microphones is reduced by almost 40% because of the central microphone, which increases the diffraction effects. In practice, the advantage of the 5-microphone-probe does not seem to be sufficiently important especially because of the increased difficulty of practical implementation, except for the case when an accurate measurement of the potential energy density (or quadratic pressure) is required.

If the performance for acoustic intensity measurements is completely independent of the standing-wave ratio, it is not the same for the determination of the energy densities. In the applications where energy densities and the intensity must be measured simultaneously, the limit must be reduced to approximately $kd = 1$.

The 6-microphone probe makes an improvement only if the pressure is averaged over all microphones. The most popular probe used that is arranged in 3 independent pairs of microphones leads to simpler formulations, but with errors much more significant in the case of the 1D field used here. To draw a final conclusion from the discussion, it will be necessary to consider more complicated fields such as the 2D fields

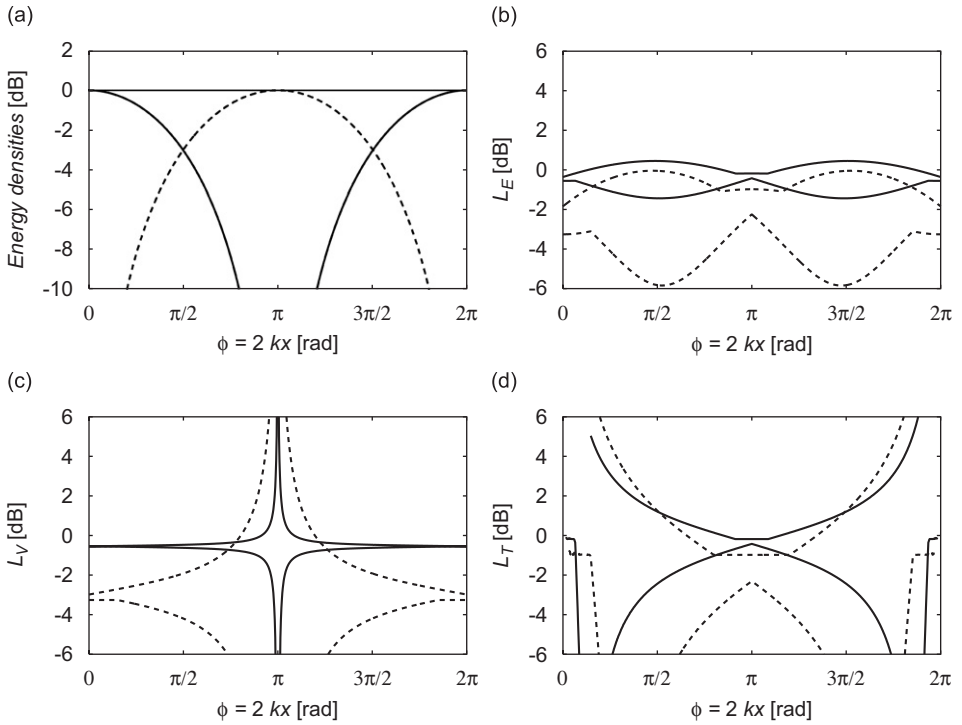

Fig. 11. Measurement errors for energy densities in a standing wave with the 4-microphone probe of the type I (4MI): (a) fluctuations of $\tilde{T}$, $\tilde{V}$ and $\tilde{E}$ along the axis of the standing wave, expressed as a function of the phase of R in Eq. (37) ($|R| = 1$). Extreme bounds of variation for: (b) total energy density $\tilde{E}$, (c) potential energy density $\tilde{V}$, (d) kinetic energy density $\tilde{T}$,—for the limit $k_L d = 2.3$ and - - - for a lower value $kd = 1$.

produced by interferences of plane waves, in which the vortex of the active intensity stream lines can be observed [18].

5. Conclusion and remarks

It is shown that the expressions for calculating the quadratic quantities for 3D probes based on the finite-sum and finite-difference approximations can easily be obtained by the use of a systematic method and symbolic computation tool independently of the probe geometry. All the energy quantities can be deduced from a *field matrix* that is calculated by this method. The examples of 3D probes consisting of 4–6 microphones illustrate the application of this method, allowing one to easily obtain the practical formulations used for measurements. The analysis of the maximum errors for the amplitude and direction angle of the intensity vector in a quasi-stationary plane wave shows that the error interval for the most popular 3D probe consisting of 6 microphones, arranged in 3 independent pairs (6M3A), is more important than that of the 4 tetrahedral microphone probes. The latter ones seem to present the best ratio of performance/cost. The errors are independent of the direction of the tetrahedron with respect to the orthogonal coordinate system. The estimate of the intensity vector is independent of the standing-wave ratio, whereas the energy densities not only depend strongly on this parameter, but also on the factor kd and the position of the probes in the field.

Appendix A. List of abbreviations used for identification of the probes

4M I tetrahedral probe with 4 microphones, the base of which is parallel to the (x, y) plane and the fourth microphone is placed on the z-axis (Figs. 1 and 2a)

4M II tetrahedral probe with 4 microphones positioned in the way that one edge is parallel to x-axis and another to y-axis (Fig. 2b)

4MV non-tetrahedral probe with 4 microphones, three of which are positioned on the axis of the Cartesian coordinates and the forth is at its origin

4MC same configuration as that of the probe 4MV, but the energy quantities are computed at the centroid

5M I tetrahedral probe with 5 microphones, four of which have an identical position to the 4M I probe and the fifth microphone placed at its centre

5M II tetrahedral probe with 5 microphones, composed of the probe 4M II and the fifth microphone placed at its centre

6M3A conventional probe with 6 microphones in which each pair of microphone aligned on one axis of the orthogonal system is treated as a 1D probe (Fig. 2c)

6MAV probe with 6 microphones whose positions are the same as those of the probe 6M3A. The spatially averaged pressure over all positions is evaluated (Fig. 2c)

Appendix B. Relations between the cross-product of the pressures at 2 microphones and the energy quantities

The cross-product between the pressure $p_i = p(\mathbf{r}_i)$ and $p_j = p(\mathbf{r}_j)$ at two points $\mathbf{r}_i$ and $\mathbf{r}_j$ can be computed by the use of the 0–2 order terms of the Taylor series expansion of Eq. (5.1) by which the pressure at each point is expressed by the pressure and its derivatives at the origin of the probe

$$\frac{1}{2}p_i p_j^* \approx \frac{1}{2}\left(p + (\mathbf{r}_i\cdot\nabla)p + \frac{1}{2}(\mathbf{r}_i\cdot\nabla)^2 p\right)\left(p^* + (\mathbf{r}_j\cdot\nabla)p^* + \frac{1}{2}(\mathbf{r}_j\cdot\nabla)^2 p^*\right). \tag{B.1}$$

Considering Eqs. (1)–(3) as well as the following expressions of the energy quantities:

$$\mathbf{\Pi} = \mathbf{I} + \mathrm{j}\mathbf{J} = \frac{1}{2}p\mathbf{u}^* = \frac{-\mathrm{j}}{2\rho_0\omega}p\nabla p^*, \tag{B.2}$$

$$\mathbf{J} = \frac{-1}{4\rho_0\omega}\nabla|p|^2, \tag{B.3}$$

$$T = T_{xx} + T_{yy} + T_{zz} = \frac{\rho_0}{4(\rho_0\omega)^2}\nabla p\cdot\nabla p^* = \frac{1}{4\rho_0\omega^2}|\nabla p|^2. \tag{B.4}$$

Eq. (B.1) can be written in the following form:

$$\begin{aligned}
\frac{1}{2}p_i p_j^* \approx\ & 2\rho_0 c^2 V - \rho_0\omega(\mathbf{r}_i+\mathbf{r}_j)\cdot\mathbf{J} - \mathrm{j}\rho_0\omega(\mathbf{r}_i-\mathbf{r}_j)\cdot\mathbf{I}\\
& - \rho_0\omega^2\left[(x_i-x_j)^2 T_{xx} + (y_i-y_j)^2 T_{yy} + (z_i-z_j)^2 T_{zz}\right]\\
& - 2\rho_0\omega^2\left[(x_i-x_j)(y_i-y_j)\mathrm{Re}\{T_{xy}\} + (y_i-y_j)(z_i-z_j)\mathrm{Re}\{T_{yz}\} + (z_i-z_j)(x_i-x_j)\mathrm{Re}\{T_{zx}\}\right]\\
& + \mathrm{j}2\rho_0\omega^2\left[(x_i y_j - x_j y_i)\mathrm{Im}\{T_{xy}\} + (y_i z_j - y_j z_i)\mathrm{Im}\{T_{yz}\} + (z_i x_j - z_j x_i)\mathrm{Im}\{T_{zx}\}\right]\\
& - \frac{1}{2}\rho_0\omega\left[(x_i^2+x_j^2)\frac{\partial J_x}{\partial x} + (y_i^2+y_j^2)\frac{\partial J_y}{\partial y} + (z_i^2+z_j^2)\frac{\partial J_z}{\partial z}\right]\\
& - \frac{\mathrm{j}}{2}\rho_0\omega\left[(x_i^2-x_j^2)\frac{\partial I_x}{\partial x} + (y_i^2-y_j^2)\frac{\partial I_y}{\partial y} + (z_i^2-z_j^2)\frac{\partial I_z}{\partial z}\right]\\
& - \frac{1}{2}\rho_0\omega\left[(x_i y_i + x_j y_j)\left(\frac{\partial J_x}{\partial y}+\frac{\partial J_y}{\partial x}\right) + (y_i z_i + y_j z_j)\left(\frac{\partial J_y}{\partial z}+\frac{\partial J_z}{\partial y}\right) + (z_i x_i + z_j x_j)\left(\frac{\partial J_z}{\partial x}+\frac{\partial J_x}{\partial z}\right)\right]\\
& - \frac{\mathrm{j}}{2}\rho_0\omega\left[(x_i y_i - x_j y_j)\left(\frac{\partial I_x}{\partial y}+\frac{\partial I_y}{\partial x}\right) + (y_i z_i - y_j z_j)\left(\frac{\partial I_y}{\partial z}+\frac{\partial I_z}{\partial y}\right) + (z_i x_i - z_j x_j)\left(\frac{\partial I_z}{\partial x}+\frac{\partial I_x}{\partial z}\right)\right]\\
& + \frac{1}{4}(\mathbf{r}_i\cdot\nabla)^2 p(\mathbf{r}_j\cdot\nabla p^*) + \frac{1}{4}(\mathbf{r}_j\cdot\nabla)^2 p^*(\mathbf{r}_i\cdot\nabla p) + \frac{1}{4}(\mathbf{r}_i\cdot\nabla)^2 p(\mathbf{r}_j\cdot\nabla)^2 p^*.
\end{aligned} \tag{B.5}$$

The last line of Eq. (B.5) corresponds to terms in $O(r^3)$ that are naturally neglected. It is noticed that the first 4 lines comprise the 16 terms constituting the real and imaginary parts of all the elements of the *field matrix*. The 6 pairs of a probe with 4 microphones lead to 12 equations (by separating the real and imaginary parts). Four other real equations are obtained by considering the expressions of $\frac{1}{2}|p_i|^2$, which can as well be calculated by putting $j=i$ in Eq. (B.5) as by using the first three terms of the Taylor series for the variable $|p(\mathbf{r}_i)|^2 = |p_i|^2$

$$\frac{1}{2}|p_i|^2 \approx \frac{1}{2}|p|^2 + \frac{1}{2}\mathbf{r}_i\cdot\nabla|p|^2 + \frac{x_i^2}{4}\frac{\partial^2|p|^2}{\partial x^2} + \frac{y_i^2}{4}\frac{\partial^2|p|^2}{\partial y^2} + \frac{z_i^2}{4}\frac{\partial^2|p|^2}{\partial z^2} + \frac{x_i y_i}{2}\frac{\partial^2|p|^2}{\partial x\,\partial y} + \frac{y_i z_i}{2}\frac{\partial^2|p|^2}{\partial y\,\partial z} + \frac{z_i x_i}{2}\frac{\partial^2|p|^2}{\partial z\,\partial x} = 2\rho_0 c^2 V - 2\rho_0 ck\mathbf{r}_i\cdot\mathbf{J} - \rho_0\omega\left[x_i^2\frac{\partial J_x}{\partial x} + y_i^2\frac{\partial J_y}{\partial y} + z_i^2\frac{\partial J_z}{\partial z} + x_i y_i\left(\frac{\partial J_x}{\partial y} + \frac{\partial J_y}{\partial x}\right) + y_i z_i\left(\frac{\partial J_y}{\partial z} + \frac{\partial J_z}{\partial y}\right) + z_i x_i\left(\frac{\partial J_z}{\partial x} + \frac{\partial J_x}{\partial z}\right)\right]. \tag{B.6}$$

To constitute a linear system of dimension 16 by 16 that can be inverted, it is necessary to neglect the terms corresponding to derivative of the components of the active and reactive intensities (lines 5–8 of Eq. (B.5)) and last line of Eq. (B.6)). All these terms can be considered as error terms, which depend on the amplitude of the spatial fluctuation of the energy fields, but also on the configuration of the microphones for the probe, knowing that the derivatives of the sound intensities are the terms composing their divergences and rotational components [7].

Appendix C. Example of approximation formulations of other energy quantities

The other energy quantities can be obtained as easily as the active intensity and the energy densities. The reactive intensity is the imaginary part of the complex intensity and is interpreted as the gradient of the quadratic pressure field [16]. To understand the role that this quantity can play in the sound field, one just needs to consider the acoustic impedance in the direction r, $Z_r = p/u_r = pu_r^*/|u_r|^2$, which can be written by using Eq. (1) in the following form:

$$\frac{Z_r}{\rho_0 c} = \frac{I_r + \mathrm{j}J_r}{2cT_{rr}}. \tag{C.1}$$

The reactive intensity is obtained from the approximations of the *field matrix*

$$\tilde{J}_x = \mathrm{Im}\{\tilde{F}_{12}\}, \quad \tilde{J}_y = \mathrm{Im}\{\tilde{F}_{13}\}, \quad \tilde{J}_z = \mathrm{Im}\{\tilde{F}_{14}\}. \tag{C.2}$$

For the 4-microphone probe of the type I (4MI), the expression (C.2) become

$$\begin{aligned}
\tilde{J}_x(\omega) &= \frac{1}{4\sqrt{3}\rho_0 ckd}[G_{11} + G_{22} - 2G_{33} - 2C_{21} - C_{31} - C_{32} + C_{41} + C_{42} - 2C_{43}]\\
\tilde{J}_y(\omega) &= \frac{1}{4\rho_0 ckd}[G_{11} - G_{22} + C_{41} - C_{42} + C_{31} - C_{32}]\\
\tilde{J}_z(\omega) &= \frac{1}{4\sqrt{6}\rho_0 ckd}[3G_{44} - G_{11} - G_{22} - G_{33} - 2(C_{21} + C_{31} + C_{32} - C_{41} - C_{42} - C_{43})]
\end{aligned} \tag{C.3}$$

and for the conventional probe with 6 microphones (6M3A), Eqs. (C.2) are written by

$$\tilde{J}_x(\omega) = \frac{G_{11} - G_{22}}{2\rho_0 ckd}, \quad \tilde{J}_y(\omega) = \frac{G_{33} - G_{44}}{2\rho_0 ckd}, \quad \tilde{J}_z(\omega) = \frac{G_{55} - G_{66}}{2\rho_0 ckd}. \tag{C.4}$$

In the same way, the curl of the active intensity vector $\mathbf{\Omega} = \nabla\times\mathbf{I}$ is obtained by the use of Eqs. (3) and (4)

$$\tilde{\Omega}_x = 2k\mathrm{Im}\{\tilde{F}_{34}\}, \quad \tilde{\Omega}_y = 2k\mathrm{Im}\{\tilde{F}_{42}\}, \quad \tilde{\Omega}_z = 2k\mathrm{Im}\{\tilde{F}_{23}\}, \tag{C.5}$$

for the 4MI probe

$$\tilde{\Omega}_x(\omega) = \frac{\sqrt{6}}{3\rho_0 ckd^2}[2Q_{21} + Q_{31} - Q_{32} - 3Q_{41} + 3Q_{42}],$$
$$\tilde{\Omega}_y(\omega) = \frac{\sqrt{2}}{\rho_0 ckd^2}[Q_{41} + Q_{42} - 2Q_{43} - Q_{31} + Q_{32}],$$
$$\tilde{\Omega}_z(\omega) = \frac{1}{\sqrt{3}\rho_0 ckd^2}[Q_{31} - Q_{32} - Q_{21}], \quad \text{(C.6)}$$

and for the 6M3A probe

$$\tilde{\Omega}_x(\omega) = \frac{2}{\rho_0 ckd^2}[Q_{53} - Q_{54} + Q_{64} - Q_{63}],$$
$$\tilde{\Omega}_y(\omega) = \frac{2}{\rho_0 ckd^2}[Q_{52} - Q_{51} + Q_{61} - Q_{62}],$$
$$\tilde{\Omega}_z(\omega) = \frac{2}{\rho_0 ckd^2}[Q_{31} - Q_{32} + Q_{41} - Q_{42}]. \quad \text{(C.7)}$$

It is these formulations that have been used in Ref. [7] for the measurement of component Ω_z in the near field of two loudspeakers.

References

[1] F.J. Fahy, Measurement of acoustic intensity using the cross-spectral density of two microphone signals, *Journal of the Acoustical Society of America* 62 (1977) 1057–1059.

[2] G. Pavic, Measurement of sound intensity, *Journal of Sound and Vibration* 51 (1977) 533–546.

[3] G.W. Elko, Frequency Domain Estimation of the Complex Acoustic Intensity and Acoustic Energy Density, PhD Thesis, Pennsylvania State University, State College, USA, 1984.

[4] B.S. Cazzolato, C.H. Hansen, Errors arising from three-dimensional energy density sensing in one-dimensional sound fields, *Journal of Sound and Vibration* 236 (2000) 375–400.

[5] B.S. Cazzolato, J. Ghan, Frequency domain expressions for the estimation of time averaged acoustic energy density, *Journal of the Acoustical Society of America* 117 (2005) 3750–3756.

[6] L.M.C. Santos, C.C. Rodrigues, J.L. Bento Coelho, Measuring the three-dimensional acoustic intensity vector with a four-microphone probe, *Proceedings of Inter-Noise 89*, Newport Beach, USA, 4–6 December 1989, pp. 965–968.

[7] J.-F. Li, J.-C. Pascal, C. Carles, Acoustic energy fields of partially coherent sources, *Journal of the Acoustical Society of America* 103 (1998) 962–972.

[8] T. Loyau, Traitement de L'information, Pour L'analyse des Champs D'intensité Acoustique et des Sources Sonores, Doctorat Thesis, Université de Technologie de Compiègne, Compiègne, France, 1988 (in French).

[9] P. Liénard, M. Bockhoff, J.-C. Pascal, J. Tourret, Intensimétrie acoustique: 2ième Congrès International, *Revue d'Acoustique* 80 (1987) 3–21 and photo of the tetrahedric probe on the cover (in French).

[10] H. Suzuki, S. Oguro, M. Anzai, T. Ono, Performance evaluation of a three dimensional intensity probe, *Journal of the Acoustical Society of Japan (E)* 16 (4) (1995) 233–238.

[11] J.S. Bendat, A.G. Piersol, *Random Data: Analysis and Measurement Procedures*, second ed., Wiley, New York, 1986.

[12] J.-C. Pascal, Intensimétrie et antennes acoustiques, in: C. Lesueur (Ed.), *Rayonnement Acoustique des Structures*, Eyrolles, Paris, 1988 (in French) (Chapter 10).

[13] F.J. Fahy, *Sound Intensity*, second ed., E & FN Spon, London, 1995.

[14] G.W. Elko, Biased against finite-difference bias, *Proceedings of Noise-Con 91*, Tarrytown (NY), USA, 14–16 July 1991, pp. 541–546.

[15] G. Rasmussen, Measurement of vector fields, *Proceedings of the Second International Congress on Acoustic Intensity*, Senlis, France, 23–26 September 1985, pp. 53–58.

[16] J.-C. Pascal, C. Carles, Systematic measurement errors with two microphone sound intensity meters, *Journal of Sound and Vibration* 83 (1982) 53–65.

[17] J. Vandenhout, P. Sas, R. Snoeys, Measurement, accuracy and interpretation of real and imaginary intensity patterns in the near field of complex radiators, *Proceedings of the Second International Congress on Acoustic Intensity*, Senlis, France, 23–26 September 1985, pp. 121–128.

[18] J.-C. Pascal, Structure and patterns of acoustic intensity fields, *Proceedings of the Second International Congress on Acoustic Intensity*, Senlis, France, 23–26 September 1985, pp. 97–104.

[19] *Matlab Symbolic Toolbox User Guide*, The Mathworks, Natick, MA, 2000.